

ARANet: Attention-based Residual Adversarial Network with Deep Supervision for Radiotherapy Dose Prediction of Cervical Cancer

Lu Wen
School of Computer Science
Sichuan University
Chengdu, Sichuan
wenlu0416@163.com

Wenxia Yin
School of Computer Science
Sichuan University
Chengdu, Sichuan
Yingwenxia@163.com

Zhenghao Feng
School of Computer Science
Sichuan University
Chengdu, Sichuan
fzh_scu@163.com

Xi Wu
School of Computer Science
Chengdu University of Information
Technology
Chengdu, Sichuan
wuxi@cuit.edu.cn

Deng Xiong
School of Computer Science
Stevens Institute of Technology
Hoboken, NJ
dxiong@stevens.edu

Yan Wang*
*Corresponding author
School of Computer Science
Sichuan University
Chengdu, Sichuan
wangyanscu@hotmail.com

Abstract—Radiation therapy is the mainstay treatment for cervical cancer, and its ultimate goal is to ensure the planning target volume (PTV) reaches the prescribed dose while reducing dose deposition of organs-at-risk (OARs) as much as possible. To achieve these clinical requirements, the medical physicist needs to manually tweak the radiotherapy plan repeatedly in a trial-and-error manner until finding the optimal one in the clinic. However, such trial-and-error processes are quite time-consuming, and the quality of plans highly depends on the experience of the medical physicist. In this paper, we propose an end-to-end Attention-based Residual Adversarial Network with deep supervision, namely ARANet, to automatically predict the 3D dose distribution of cervical cancer. Specifically, given the computer tomography (CT) images and their corresponding segmentation masks of PTV and OARs, ARANet employs a prediction network to generate the dose maps. We also utilize a multi-scale residual attention module and deep supervision mechanism to enforce the prediction network to extract more valuable dose features while suppressing irrelevant information. Our proposed method is validated on an in-house dataset including 54 cervical cancer patients, and experimental results have demonstrated its obvious superiority compared to other state-of-the-art methods.

Keywords—Radiation Therapy, Dose Prediction, Residual Attention Network, Deep Supervision

I. INTRODUCTION

As one of the main methods of cancer treatment, radiotherapy aims to maximize the treatment-gain ratio. This means ensuring that the prescribed tumor volume (PTV) receives the specified dose of radiation with adequate coverage while minimizing unnecessary radiation exposure to the organs-at-risk (OARs). With the development of intensity modulated radiation therapy (IMRT) and volume modulated arc therapy (VMAT), the overall quality of the radiotherapy plan has been improved rapidly [1], [2]. However, designing a clinically acceptable treatment plan is still a complicated and

extremely time-consuming process, which is highly dependent on the experience of medical physicists [3], [4]. One solution for this limitation is to automatically predict the dose distribution of radiotherapy by extracting knowledge from existing plans, thereby providing the standard for dosimetry verification and quality control of future radiotherapy plans [5-7].

Existing dose distribution prediction methods of radiotherapy planning can be roughly divided into two categories: knowledge-based planning (KBP) [8], [9] and deep neural network (DNN)-based planning [10-14]. Generally speaking, KBP methods take the treatment plans of historical patients as references and perform dosimetric predictions for new patients. To be specific, these methods first build a mathematical model for the historical dose information of existing patients and then apply the generated model to predict the dose distribution for new patients. However, these KBP methods highly rely on the handcrafted features corresponding to the dose distribution results, i.e., overlapping volume histogram (OVH), distance-to-target histogram (DTH), and dose volume histogram (DVH), which also come from the manual procedures of feature extraction [15-17].

In recent years, inspired by the great success of deep learning [18-22], DNNs have been successfully applied to predict the dose distribution in radiotherapy [23-26]. For instance, Kearney *et al.* [23] proposed a DoseNet based on U-net to obtain dose maps efficiently. Song *et al.* [24] designed a flexible framework based on the deep neural network DeepLabv3+, achieving the automatic prediction of dose maps. Nguyen *et al.* [25] applied the U-net and DenseNet framework to the dose prediction task and realized the radiotherapy dose planning of the head and neck (H&N) cancer automatically. Compared with the knowledge-based methods, these DNN-based works directly train end-to-end deep models from the historical plans without physicist intervention. Based on the

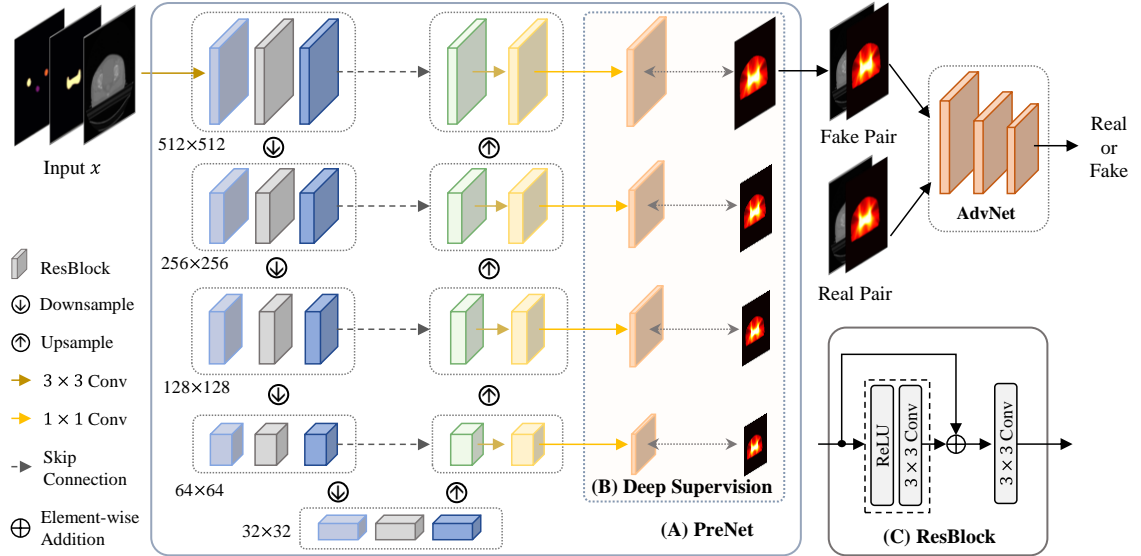


Fig. 1. Illustration of our proposed ARANet which contains a multi-scale residual attention network and a deep supervision mechanism.

automatically learned features using the deep model, this kind of method can achieve a more effective automatic prediction with relatively high prediction accuracy.

In this paper, we develop a 3D dose prediction framework based on an end-to-end residual attention adversarial network with deep supervision, namely ARANet. Fed with CT images and corresponding segmentation masks of PTV and OARs, ARANet can automatically output the dose distribution of cervical cancer. Our contributions can be summarized as:

- Due to the remarkable progress of generative adversarial networks (GANs), the proposed method takes account of an adversarial network (AdvNet), enforcing the prediction network (PreNet) to generate dose maps similar to the real ones.
- To adaptively integrate the valuable dose features while suppressing irrelevant information, a multi-scale residual attention network combined with a deep supervision mechanism is proposed as the generator of GANs.
- Both the quantitative and qualitative experimental results show that our method outperforms the state-of-the-art dose prediction methods.

II. RELATED WORKS

A. Knowledge-Based Planning Methods

Knowledge-based planning has made great progress in radiotherapy plans. It predicts the dose distribution of new patients with a set of existing historical plans of treated patients for reference. Based on the indication of dose volume histogram (DVH), Wu *et al.* [15] proposed a new concept, i.e., overlap volume histogram (OVH) which has a strong correlation with DVH. Under the guidance of clinical experience, it was supposed that the farther the distance from the PTV, the lower dose of voxel. Obeying this hypothesis, the corresponding upper (lower) limit can be found according to the OVH comparison of a certain organ. Consequently, the new patient can obtain the DVH prediction of a certain organ by substituting the DTH to the correlation model. To a certain extent, this method can get a good prediction result. However,

such knowledge-based methods are prone to two limitations. The first one is that they ignore the three-dimensional spatial information of medical images since the DVH or DTH is the embodiment of two-dimensional information. The second one is that they require much effort and time from medical physicists to determine the applicable handcrafted features to obtain a good prediction result.

B. DNN-based Planning Methods

Recent research on 3D dose distribution prediction is mostly based on deep neural networks. Specifically, Nguyen *et al.* [25] proposed a new model named hierarchically densely connected U-net (HD U-net) to predict the dose distribution. Specifically, 3D image patches were fed into a U-net framework that integrates dense connecting blocks achieving satisfactory experimental results. Kearney *et al.* [23] presented a prediction model called DoseNet to predict the dose distribution of prostate cancer patients. DoseNet was a fully convolutional neural network based on U-net which accepts six three-dimensional matrices as inputs to the first convolution layer, including three-dimensional CT images of the prostate, bladder, bulbar penis, urethra, and rectum. All input channels were normalized as six separate groups before training. DoseNet finally outputs the prediction results of radiotherapy dose distribution of the patients. Song *et al.* [24] applied the DeepLabv3+ framework to the dose prediction task of rectal cancer. In this work, an atrous spatial pyramid pooling module is used to extract features, and the loss function is defined by mean square error. To address the gradient vanishing problem, Fan *et al.* [26] proposed a dose prediction scheme based on ResNet, and demonstrated that deep learning methods are beneficial to clinical applications, as the quality and efficiency of treatment planning for radiotherapy are improved.

III. METHODOLOGY

A. Architecture

The overview of our framework is illustrated in Fig.1 which considers the generative adversarial network as the backbone, including a generator (PreNet) and a discriminator (AdvNet). To extract valuable dose features while suppressing irrelevant information, a multi-scale residual attention module is designed in the PreNet. Also, to speed up the convergence process and

improve prediction accuracy, a deep supervision mechanism is integrated with PreNet. On the whole, in the training stage, the original CT images, segmentation images of OARs (including bladder, left and right femur, small intestine), and PTV are fed into the neural network. With the help of the competition between the AdvNet and the PreNet, we can finally get a trained-well model that can output a predicted 3D dose distribution image of cervical cancer patients. In the test stage, we only need the trained model to predict new cases and discard the AdvNet. Please note that, the clinically acceptable dose distribution images which are marked by the physicists are regarded as the ground truth for network training.

B. PreNet

For the PreNet, we first concatenate the slices of 3D CT, OARs, and PTV with the size of 512×512 and input them into the encoding path of the U-net-like network. After a 3×3 kernel with a stride of 1, a $16 \times 512 \times 512$ feature map is obtained, which will be further processed by a residual convolution module (shown in Fig. 1(c)) to get a refined result. The refined feature representation is integrated by both high- and low-level features and has the same size as the previous one. Then we take the down-sampling operation to decrease the scale of the feature map while increasing the number of channels by a factor of 2. After the four above-mentioned operations, we can finally obtain an encoded deep feature with the size of 64×64 . To map the encoded feature to the dose map space, it will be fed into a decoding path. Going through four upsampling operations, the encoded deep feature can be eventually restored to the same size as input images.

C. Spatial Attention Mechanism

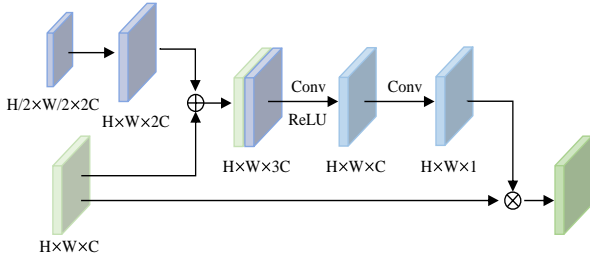


Fig. 2. Illustration of spatial attention mechanism inside the skip connections.

As shown in Fig. 2, we use skip connections with a spatial attention mechanism to fuse the lower-layer encoding features with the corresponding higher-layer decoding features during each upsampling stage. Specifically, the decoding deep feature is upsampled to a certain scale that is consistent with the encoding feature, and then cascaded with the encoding feature along the channel direction. After two consecutive convolution layers, the cascaded feature is turned into an attention map, which is leveraged to perform element-wise multiplication with the encoding feature in each channel, thus producing the upper-layer decoding feature. Furthermore, to get a more precise result, we apply 1×1 kernels to acquire coarse predictions at each scale and enforce them to be supervised by the real dose map rescaled to the corresponding size, which is called a deep supervision mechanism.

D. Loss Functions

The total loss function L_{total} for network optimization is comprised of two parts: (1) L_{pre} for the PreNet training, and (2) L_{adv} for the AdvNet training. L_{total} can be written as below:

$$L_{total} = \lambda_1 L_G + \lambda_2 L_{adv}, \quad (1)$$

where λ_1 and λ_2 are two hyper-parameters to balance the two terms.

Concretely, L_{pre} in Equation (2) contains the deep supervision loss L_{DS} and the loss L_{final} between the final predicted dose map and the ground truth.

$$L_G = L_{final} + \lambda_3 L_{DS}, \quad (2)$$

where λ_3 is a weighted hyper-parameters

As formulated in Equation (3), L_{DS} is a commonly used mean squared error (MSE) loss that supervises the deep predictions at three scales to resemble the ground truth:

$$L_{DS}(y_i, y_i^p) = \sum_{i=1}^3 (y_i - y_i^p)^2, \quad (3)$$

where y_i^p represents the predicted dose distribution map at i -th supervised scale and y_i is the corresponding ground truth at i -th scale.

L_{final} is a smooth L1 loss which can be expressed as Equation (4), ensuring that the final predicted dose map $G(x)$ stay as close to the real dose map y as possible:

$$L_{final}(y, f(x)) = \begin{cases} \frac{1}{2} (y - G(x))^2, & |y - G(x)| < \delta \\ \delta (|y - G(x)| - \frac{1}{2} \delta), & |y - G(x)| \geq \delta \end{cases}, \quad (4)$$

where δ represents a prediction error.

Meanwhile, to obtain a more precise result, the AdvNet D takes the adversarial loss for the objective function, which is defined in Equation (5):

$$L_{adv}(D, G) = E(D(y)) + E(1 - D(G(x))). \quad (5)$$

IV. EXPERIMENTS

A. Dataset

To validate the performance of the proposed network, we use an in-house clinical cervical cancer dataset with 54 cases who have taken the VAMT plan in West China Hospital, Sichuan University, Chengdu, China. For each case, the CT scan and corresponding segmentation mask of OARs are included. Specifically, the OARs of cervical cancer contain bladder, left and right femur, small intestine, and rectum. For data partition, we randomly select 40, 6, and 8 cases for model training, validation, and testing, respectively.

B. Dosimetric evaluation metrics

To objectively evaluate the results of the proposed dose prediction model, we calculate the normalized average percent prediction error (APE) to measure the difference between the metrics of ground truth and prediction. The mathematical definition is shown in Equation (6).

$$\Delta = \frac{1}{n} \sum_{i=1}^n \frac{|Truth_i - Prediction_i|}{Prediction_i} \times 100\%. \quad (6)$$

Simultaneously, following [25], we use the conformity index (CI) and heterogeneity index (HI) to evaluate the dosimetric distribution inside the PTV areas between the

TABLE I. QUANTITATIVE COMPARISON WITH SOTA METHODS IN TERMS OF PTV D_{mean} AND PTV V₅₀, RESPECTIVELY. THE BEST RESULTS ARE IN **BOLD**.

Patient	PTV Dmean (Gy)					PTV V ₅₀				
	Original	Proposed	ResNet	DoseNet	DeepLabv3+	Original	Proposed	ResNet	DoseNet	DeepLabv3+
P1	45.76	46.17(0.41)	51.29(5.53)	45.98(0.22)	48.75(3.00)	0.13	0.18(0.04)	0.94(0.80)	0.74(0.60)	0.66(0.52)
P2	45.33	45.80(0.48)	51.19(5.87)	45.17(0.15)	47.94(2.61)	0.06	0.08(0.02)	0.94(0.89)	0.27(0.21)	0.65(0.60)
P3	45.64	45.91(0.27)	51.96(6.32)	44.74(0.90)	49.15(3.51)	0.05	0.08(0.02)	0.99(0.94)	0.00(0.05)	0.58(0.53)
P4	45.80	46.26(0.28)	51.30(5.32)	45.44(0.54)	48.98(3.00)	0.07	0.08(0.01)	0.96(0.89)	0.66(0.60)	0.74(0.67)
P5	45.41	45.63(0.22)	51.98(6.57)	45.21(0.20)	48.90(3.50)	0.02	0.02(0.00)	0.99(0.97)	0.00(0.01)	0.48(0.46)
P6	53.38	53.30(0.09)	51.97(1.41)	46.13(7.25)	48.97(4.41)	0.98	0.98(0.00)	0.99(0.00)	0.6(0.39)	0.74(0.25)
P7	45.99	46.19(0.20)	51.30(5.31)	45.55(0.43)	48.26(2.27)	0.11	0.16(0.05)	0.93(0.81)	0.37(0.26)	0.56(0.45)
P8	52.72	51.16(1.55)	51.92(0.79)	44.86(7.86)	49.65(3.06)	0.96	0.80(0.17)	0.97(0.00)	0.43(0.54)	0.85(0.11)
Avg	48.00	47.55(0.03)	51.61(4.09)	45.38(2.13)	48.82(1.30)	0.30	0.30(0.00)	0.96(0.67)	0.38(0.09)	0.66(0.34)

TABLE II. QUANTITATIVE COMPARISON WITH SOTA METHODS IN TERMS OF CONFORMITY INDEX (CI) AND HETEROGENEITY INDEX (HI), RESPECTIVELY.

Patient	CI					HI				
	Original	Proposed	ResNet	DoseNet	DeepLabv3+	Original	Proposed	ResNet	DoseNet	DeepLabv3+
P1	0.72	0.78(0.06)	0.58(0.14)	0.78(0.06)	0.71(0.02)	0.29	0.21(0.08)	0.12(0.17)	0.13(0.16)	0.16(0.13)
P2	0.81	0.83(0.02)	0.53(0.28)	0.78(0.04)	0.71(0.10)	0.25	0.18(0.07)	0.11(0.14)	0.13(0.12)	0.15(0.10)
P3	0.86	0.88(0.02)	0.59(0.27)	0.64(0.22)	0.72(0.13)	0.23	0.13(0.11)	0.08(0.15)	0.15(0.09)	0.13(0.10)
P4	0.86	0.86(0.00)	0.64(0.22)	0.82(0.04)	0.73(0.13)	0.25	0.17(0.08)	0.10(0.14)	0.11(0.14)	0.14(0.11)
P5	0.79	0.80(0.01)	0.57(0.22)	0.79(0.00)	0.71(0.09)	0.15	0.16(0.01)	0.08(0.07)	0.11(0.04)	0.13(0.02)
P6	0.64	0.56(0.08)	0.57(0.06)	0.82(0.18)	0.69(0.06)	0.09	0.12(0.03)	0.08(0.00)	0.12(0.04)	0.12(0.03)
P7	0.73	0.69(0.05)	0.55(0.19)	0.72(0.01)	0.69(0.05)	0.29	0.25(0.04)	0.12(0.17)	0.16(0.13)	0.18(0.11)
P8	0.68	0.74(0.05)	0.68(0.02)	0.71(0.03)	0.73(0.05)	0.10	0.12(0.02)	0.10(0.00)	0.11(0.01)	0.12(0.02)
Avg	0.76	0.77(0.004)	0.59(0.17)	0.76(0.01)	0.71(0.05)	0.20	0.17(0.04)	0.01(0.11)	0.13(0.08)	0.14(0.06)

TABLE III. QUANTITATIVE COMPARISON WITH SOTA METHODS IN TERMS OF BLADDER D_{mean} .

Patient	Bladder Dmean%(Gy)									
	Original	Proposed	ResNet	Dosenet	Deeplabv3+	Δ Proposed	Δ ResNet	Δ Dosenet	Δ Deeplabv3+	
P1	23.929	24.560	27.998	27.745	26.971	0.631	4.069	3.816	3.042	
P2	28.768	30.207	36.555	34.800	32.722	1.439	7.787	6.032	3.954	
P3	25.433	26.699	32.364	32.730	29.832	1.266	6.931	7.297	4.399	
P4	31.201	32.254	36.090	32.798	34.008	1.053	4.889	1.597	2.807	
P5	28.322	28.738	34.879	32.408	31.514	0.416	6.557	4.086	3.192	
P6	33.972	36.992	33.678	31.875	32.463	3.02	0.294	2.097	1.509	
P7	34.757	29.882	31.816	31.473	30.374	4.875	2.941	3.284	4.383	
P8	39.151	35.820	36.317	35.693	37.153	3.331	2.834	3.458	1.998	
Avg	30.691	30.644	33.712	32.44	31.879	0.047	3.02	1.749	1.188	

predicted dose distribution map and the ground truth. Among them, CI is formulated as Equation (7), where TV is the target volume, PIV is the prescription isodose volume.

$$CI = (TV \cap PIV)^2 / (TV \times PIV). \quad (7)$$

HI formalism is defined as Equation (8), where D_m is the minimal absorbed dose covering $m\%$ percentage volume of PTV.

$$HI = (D_2 - D_{98}) / D_{50}. \quad (8)$$

Since V_x denotes the percentage volume that receives a dose level of at least x , we also utilize V_{50} as another metric for dose evaluation.

C. Training Details

The proposed method is implemented with the PyTorch framework and all experiments are conducted on a single NVIDIA GeForce RTX 3090 GPU equipped with 24GB of memory. The training phase is executed with a batch size of 16. The whole model is trained for 100 epochs where the learning rate is set as $1e-5$. An adaptive moment estimation (Adam) optimizer is exploited to facilitate an efficient convergence. As for hyper-parameter λ_1 , λ_2 , and λ_3 , according to the previous experience, we set them as 2, 1, and 0.5 respectively.

D. Comparison with State-of-the-art (SOTA) Methods

To investigate the superiority of our proposed ARA-Net, we take several SOTA methods into consideration for comparison: (1) ResNet [26], (2) DoseNet [23], and (3) DeepLabv3+ [24]. The quantitative comparison results are summarized in Table I, Table II, and Table III, respectively. Specifically, Table I shows the D_{mean} values and V_{50} values of PTV generated by various methods, where P_i represents i -th patient and the values in parentheses represent the difference between the predicted and ground truth. V_{50} denotes the percentage volume that receives a dose level of at least 50. Table II shows the conformity index (CI) and heterogeneity index (HI) compared with the existing methods.

Table I and Table II show the results of indicators on PTV. Compared with other methods, our ARA-Net achieves the best scores on all clinical metrics. Specifically, as displayed in Table I, the proposed method gains 47.55 Gy and 0.30 in terms of D_{mean} and V_{50} , which are highly approximated to those of the ground truth, i.e., 48.00 Gy and 0.30. Furthermore, in Table II, such superior performance can also be observed in terms of CI, and HI. To more comprehensively evaluate the performance of the proposed method, we show the prediction results on the bladder in terms of D_{mean} in Table III. As seen, our method also achieves the best prediction, i.e., 30.644 Gy, with the least error, i.e., 0.047 Gy.

TABLE IV. ABLATION EXPERIMENT RESULTS IN TERMS OF PTV D_{mean} .

Patient	PTV D_{mean} (Gy)								
	Original	Proposed	U-net	AU-net	RAU-net	Δ Proposed	Δ U-Net	Δ AU-Net	Δ RAU-Net
P1	45.76	46.17	50.77	46.15	47.25	0.41	5.02	0.39	1.50
P2	45.32	45.80	49.69	43.57	46.13	0.48	4.36	1.76	0.80
P3	45.64	45.91	49.80	45.96	45.64	0.27	4.16	0.33	0.00
P4	45.98	46.26	49.24	43.79	47.29	0.28	3.26	2.19	1.31
P5	45.41	45.63	49.59	44.39	47.32	0.22	4.19	1.02	1.91
P6	53.38	53.30	50.91	46.36	47.68	0.09	2.48	7.03	5.70
P7	45.99	46.19	49.87	44.06	45.99	0.20	3.89	1.93	0.00
P8	52.72	51.16	50.55	45.81	48.71	1.55	2.17	6.91	4.00
Avg	47.52	47.55	50.05	45.01	47.00	0.03	2.53	2.51	0.52

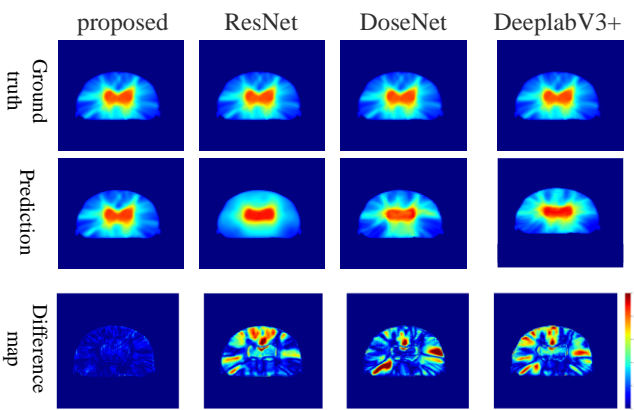


Fig. 3. Visualization results compared with SOTA methods. The first row is ground truth, the second and the last rows are dose distribution prediction results and corresponding difference maps respectively.

On the other hand, for qualitative comparison, we provide the dose maps predicted by different methods as well as corresponding difference maps in Fig. 3. It is obvious that the result of our method is the closest to ground truth, especially for the radial pattern and the planning region of dose distribution. The fact that the difference map of our method is darkest also supports the above conclusion.

Based on all these experimental results, we can gain the conclusion that our method achieves superior performance both quantitatively and qualitatively.

E. Ablation experiments

To evaluate the effectiveness of every module in ARA-Net. A series of ablation experiments are conducted. The experimental arrangements can be summarized as: (A) U-Net with deep supervision as backbone (denoted as U-Net); (B) U-Net + adversarial training (denotes as AU-Net); and (C) AU-Net + residual attention (denotes as RAU-Net). Corresponding experimental results are exhibited in Fig. 4, Table IV, and Table V. Table IV shows the results of experiments on D_{mean} of PTV. As seen, with the addition of residual attention, the prediction in terms of D_{mean} is enhanced from 45.01 Gy to 47.00 Gy. The average percent prediction error is shown in Table V. Especially in Table V when combining all the designed modules, our method reduces the prediction error of D_{50} to $0 \pm 0.007\%$.

Fig. 4 shows the visualization results of ablation experiments. Specifically, the predicted dose distribution map is extremely similar to the ground truth demonstrating the accuracy of the proposed method.

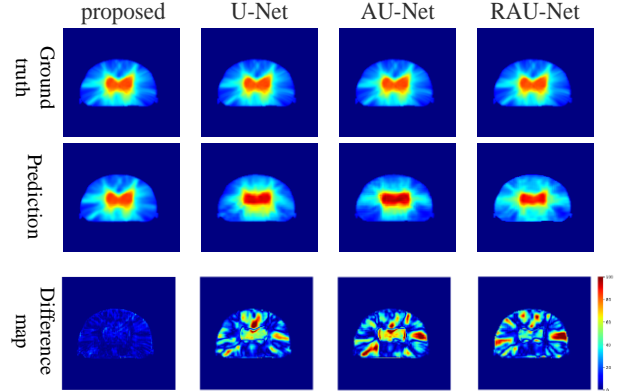


Fig. 4. Visualization results of ablation experiments. The first rows are ground truth, the second and last rows are dose distribution prediction results and difference maps respectively.

TABLE V. AVERAGE PERCENT PREDICTION ERROR.

Method	D_{95}	D_{50}	D_{mean}
U-net	0.074 \pm 0.042	0.054 \pm 0.057	0.045 \pm 0.051
AU-net	0.033 \pm 0.050	0.03 \pm 0.055	0.05 \pm 0.049
RAU-net	0.020 \pm 0.038	0.006 \pm 0.058	0.01 \pm 0.047
Proposed	0.007\pm0.033	0.000\pm0.007	0.000\pm0.011

In a nutshell, with the gradual addition of key components, the prediction performance is nearly progressively enhanced, verifying the positive impact of our proposed modules.

V. CONCLUSION

In this paper, we have proposed a novel residual attention adversarial network combined with deep supervision namely ARA-Net, which can be used to predict the dose distribution of cervical cancer from CT images automatically. Owing to the residual convolution module that can extract more detailed features and the attention module that can make full use of features in different channels, we can acquire a prediction dose map that is highly consistent with the real dose distribution without human intervention. Besides, by using deep supervision, we can further refine the predicted dose map to achieve a clinically acceptable level. All the conducted experiments prove that our ARA-Net is advanced in automatic dose distribution prediction.

ACKNOWLEDGMENT

This work is supported by National Natural Science Foundation of China (NSFC 62371325, 62071314), Sichuan Science and Technology Program 2023YFG0263, 2023YFG0025, 2023YFG0101.

REFERENCES

- [1] Z. Jiao et al., "TransDose: Transformer-based Radiotherapy Dose Prediction from CT Images guided by Super-Pixel-Level GCN Classification," *Medical Image Analysis*, p. 102902, Oct. 2023, doi: 10.1016/j.media.2023.102902.
- [2] B. Zhan et al., "Multi-constraint generative adversarial network for dose prediction in radiotherapy," *Medical Image Analysis*, p. 102339, Apr. 2022, doi: 10.1016/j.media.2021.102339.
- [3] F. Fukuyama, "The great disruption: human nature and the reconstitution of social order," *Choice Reviews Online*, vol. 37, no. 03, pp. 37-1616-37-1616, Nov. 1999, doi: 10.5860/choice.37-1616.
- [4] B. Wu, D. Pang, P. Simari, R. Taylor, G. Sanguineti, and T. McNutt, "Using overlap volume histogram and IMRT plan data to guide and automate VMAT planning: A head-and-neck case study," *Medical Physics*, vol. 40, no. 2, p. 021714, Jan. 2013, doi: 10.1118/1.4788671.
- [5] R. Gao, B. Lou, Z. Xu, D. Comaniciu, and A. Kamen, "Flexible-C(\(\backslash\mboxm\)) GAN: Towards Precise 3D Dose Prediction in Radiotherapy," in *IEEE/CVF Conference on Computer Vision and Pattern Recognition*, CVPR 2023, Vancouver, BC, Canada, June 17-24, 2023, IEEE, 2023, pp. 715-725. doi: 10.1109/CVPR52729.2023.00076.
- [6] L. Wen et al., "A Transformer-Embedded Multi-Task Model for Dose Distribution Prediction," *International Journal of Neural Systems*, Aug. 2023, doi: 10.1142/s0129065723500430.
- [7] H. Li et al., "Explainable attention guided adversarial deep network for 3D radiotherapy dose distribution prediction," *Knowledge-Based Systems*, vol. 241, p. 108324, Apr. 2022, doi: 10.1016/j.knsys.2022.108324.
- [8] B. Wu et al., "An OVH-driven Automated IMRT Treatment Planning System," *International Journal of Radiation Oncology, Biology, Physics*, vol. 78, no. 3, p. S187, Nov. 2010, doi: 10.1016/j.ijrobp.2010.07.455.
- [9] B. Wu et al., "Data-driven approach to generating achievable dose-volume histogram objectives in intensity-modulated radiotherapy planning," *International journal of radiation oncology, biology, physics*, vol. 79 4, pp. 1241-7, 2011.
- [10] Z. Feng et al., "DiffDP: Radiotherapy Dose Prediction via a Diffusion Model," in *International Conference on Medical Image Computing and Computer-Assisted Intervention (MICCAI 2023)*, Cham: Springer Nature Switzerland, 2023, pp. 191-201.
- [11] L. Wen et al., "Multi-level Progressive Transfer Learning for Cervical Cancer Dose Prediction," *Pattern Recognition*, p. 109606, Sep. 2023, doi: 10.1016/j.patcog.2023.109606.
- [12] Z. Feng et al., "Diffusion-based Radiotherapy Dose Prediction Guided by Inter-slice Aware Structure Encoding," *arXiv preprint arXiv:2311.02991*, Nov. 2023.
- [13] L. Wen et al., "Triplet-constraint Transformer with Multi-scale Refinement for Dose Prediction in Radiotherapy," *arXiv preprint arXiv:2402.04566*.
- [14] L. Wen et al., "DoseTransfer: A Transformer Embedded Model With Transfer Learning for Radiotherapy Dose Prediction of Cervical Cancer," *IEEE Transactions on Radiation and Plasma Medical Sciences*, vol. 8, no. 1, p. 95-104, Nov. 2023, doi: 10.1109/TRPMS.2023.3330772.
- [15] Wu et al., "Fully Automated Simultaneous Integrated Boosted-Intensity Modulated Radiation Therapy Treatment Planning Is Feasible for Head-and-Neck Cancer: A Prospective Clinical Study," *International Journal of Radiation Oncology*Biolog*Physics*, vol. 84, no. 5, pp. e647-e653, Dec. 2012, doi: 10.1016/j.ijrobp.2012.06.047.
- [16] A. K. Kaskel, R. Zeiser, R. Jochim, W. Schultze-Seemann, C. Waller, and H. Veelken, "Vaccination of Advanced Prostate Cancer Patients with PSCA and PSA Peptide-Loaded Dendritic Cells Induces Cellular Immune Responses That Correlate with Superior Overall Survival.," *Blood*, vol. 106, no. 11, p. 2394, Nov. 2005, doi: 10.1182/blood.V106.11.2394.2394.
- [17] P. Carrasco, N. Jornet, A. Latorre, T. Eudaldo, A. Ruiz, and M. Ribas, "3D DVH-based metric analysis versus per-beam planar analysis in IMRT pretreatment verification," *Medical Physics*, vol. 39, no. 8, Aug. 2012, doi: 10.1118/1.4736949.
- [18] X. Zheng, T. Sang, R. Chen, and Z. Zeng, "Enhancing Semiconductor Chip Image Defect Classification Using Deep Learning and Segmented Defect Region Information," in *2023 IEEE International Conference on Cybernetics and Intelligent Systems (CIS) and IEEE Conference on Robotics, Automation and Mechatronics (RAM)*, 2023, pp. 204-209. doi: 10.1109/CIS-RAM55796.2023.10370751.
- [19] Z. Zhou, X. Zheng, Q. Han, W. Zhao, T. Sang, and Z. Zeng, "Improved Semantic Segmentation Adversarial Networks Applied to Industrial Production Datasets," in *2023 IEEE International Conference on Cybernetics and Intelligent Systems (CIS) and IEEE Conference on Robotics, Automation and Mechatronics (RAM)*, 2023, pp. 174-179. doi: 10.1109/CIS-RAM55796.2023.10370747.
- [20] P. Tiyajamorn et al., "Automatic Trash Classification using Convolutional Neural Network Machine Learning," in *2019 IEEE International Conference on Cybernetics and Intelligent Systems (CIS) and IEEE Conference on Robotics, Automation and Mechatronics (RAM)*, 2019, pp. 71-76. doi: 10.1109/CIS-RAM47153.2019.9095775.
- [21] H. Hu, P. Li, and Y. Chen, "Bitern-based multilayer perceptron network for tagging short text," in *2015 IEEE 7th International Conference on Cybernetics and Intelligent Systems (CIS) and IEEE Conference on Robotics, Automation and Mechatronics (RAM)*, 2015, pp. 212-217. doi: 10.1109/ICCIS.2015.7274575.
- [22] L. Wen et al., "Dcl-Net: Dual Contrastive Learning Network for Semi-Supervised Multi-Organ Segmentation," in *ICASSP 2024-2024 IEEE International Conference on Acoustics, Speech and Signal Processing (ICASSP)*, IEEE, pp. 1876-1880.
- [23] V. Kearney, J. W. Chan, S. Haaf, M. Descovich, and T. D. Solberg, "DoseNet: a volumetric dose prediction algorithm using 3D fully-convolutional neural networks," *Physics in Medicine & Biology*, vol. 63, no. 23, p. 235022, Dec. 2018, doi: 10.1088/1361-6560/aaef74.
- [24] Y. Song et al., "Dose prediction using a deep neural network for accelerated planning of rectal cancer radiotherapy," *Radiotherapy and Oncology*, pp. 111-116, Aug. 2020, doi: 10.1016/j.radonc.2020.05.005.
- [25] D. Nguyen et al., "3D radiotherapy dose prediction on head and neck cancer patients with a hierarchically densely connected U-net deep learning architecture," *Physics in Medicine & Biology*, vol. 64, no. 6, p. 065020, Mar. 2019, doi: 10.1088/1361-6560/ab039b.
- [26] J. Fan, J. Wang, Z. Chen, C. Hu, Z. Zhang, and W. Hu, "Automatic treatment planning based on three-dimensional dose distribution predicted from deep learning technique," *Medical Physics*, pp. 370-381, Jan. 2019, doi: 10.1002/mp.13271.